THE JOURNAL OF PHYSICAL CHEMISTRY LETTERS
A JOURNAL OF THE AMERICAN CHEMICAL SOCIETY

pubs.acs.org/JPCL

Letter

Ligand Dynamics Time Scales Identify the Surface–Ligand Interactions in Thiocyanate-Capped Cadmium Sulfide Nanocrystals

Samadhan H. Deshmukh, Srijan Chatterjee, Deborin Ghosh,* and Sayan Bagchi*

Cite This: *J. Phys. Chem. Lett.* 2022, 13, 3059–3065

Read Online

ACCESS | Metrics & More | Article Recommendations | Supporting Information

ABSTRACT: The nanocrystal surface, which acts as an interface between the semiconductor lattice and the capping ligands, plays a significant role in the attractive photophysical properties of semiconductor nanocrystals for use in a wide range of applications. Replacing the long-chain organic ligands with short inorganic variants improves the conductivity and carrier mobility of nanocrystal-based devices. However, our current understanding of the interactions between the inorganic ligands and the nanocrystals is obscure due to the lack of experiments to directly probe the inorganic ligands. Herein, using two-dimensional infrared spectroscopy, we show that the variations in the inorganic ligand dynamics within the heterogeneous nanocrystal ensemble can identify the diversities in the inorganic ligand–nanocrystal interactions. The ligand dynamics time scale in SCN^- capped CdS nanocrystals identifies three distinct ligand populations and provides molecular insight into the nanocrystal surface. Our results demonstrate that the SCN^- ligands engage in a dynamic equilibrium and stabilize the nanocrystals by neutralizing the surface charges through both direct binding and electrostatic interaction.

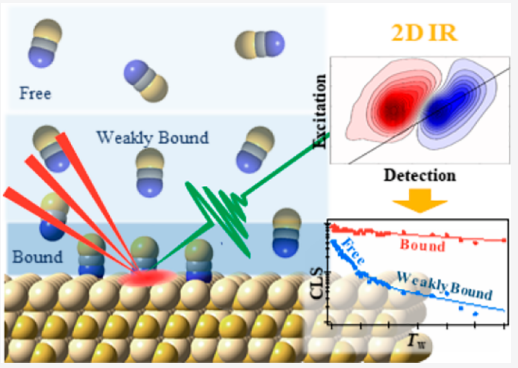

Semiconductor nanocrystals (NCs) are composed of a semiconductor lattice whose surface is passivated with molecular capping ligands. Selection of the capping ligands, semiconductor material, size, and dimension provides highly tunable optical and electronic properties of the NCs. These characteristics make the NCs an emerging class of building blocks in various optoelectronic, photovoltaic, photocatalytic, and biodiagnostic applications.[1−7] The last few decades have witnessed advances in controlling the reproducibility of size and shape dispersity in NC synthesis.[8] However, one of the most defining features of the properties and reactivity of the NCs is the surface, which acts as an interface between the semiconductor lattice and the capping ligands.[9] Unlike conventional molecules, heterogeneity exists across the surface of an individual NC. In addition, a dynamic equilibrium exists between the ligands bound to the NC surface and the free ligands in the surrounding media.[8,10] Detailed insight into the heterogeneity in ligand–NC interactions is essential to improve the current NC-based technologies.

Long-chain organic ligands are usually used for stabilizing NCs during their preparation. However, replacing the long-chain ligands with shorter variants improves the conductivity and carrier mobility, thereby increasing NC-based device performance.[11−14] In the past decade, solution-based ligand exchange has routinely been used to replace the long-chain organic ligands with the shorter inorganic variants (e.g., halides, pseudohalides, azides, halometalates).[15−17] Thiocyanate (SCN^-) ligand has been recently utilized to prepare colloidal quantum ink, which showed superior carrier mobility.[15] Despite the importance of the NC surface, the heterogeneous ligand–NC interactions are poorly understood due to a lack of molecular-level information.[8] ^{1}H NMR has recently been utilized for long-chain organic ligands (acids and thiolates) to distinguish between surface-bound and freely diffusing ligands.[8,9,18−23] However, ^{1}H NMR cannot be applied to short inorganic pseudohalide ligands like thiocyanates which are devoid of hydrogen atoms. The interactions of these short ligands at the NC surfaces have been qualitatively explained based on the hard and soft acids and bases (HSAB) principle.[9,16] However, a recent quantum chemical study has reported that the coordination of the SCN^- ligand only partly follows the HSAB principle, which cannot be generalized to inorganic solid materials.[24] Quantitative information on the binding modes and the coordination number of inorganic ligands is required to understand their influence on the NC properties.

The use of Fourier transform infrared (FTIR) and Raman spectroscopies has been reported to access purity, ligand identity, and static coordination environments at the NC surface.[15,21,25] Although most of the ligands (both long chain

Received: February 18, 2022
Accepted: March 25, 2022
Published: March 30, 2022

https://doi.org/10.1021/acs.jpclett.2c00493
J. Phys. Chem. Lett. 2022, 13, 3059–3065

acids and short pseudohalides) have distinct vibrational signatures, these steady-state vibrational techniques are most helpful in understanding ligand−NC interactions when used in complement with other experiments and quantum calculations. Beyond probing the static coordination environments, transient IR (TRIR) spectroscopy has been successfully used for the long-chain oleic acid ligands.[26,27] However, no time-resolved IR studies have been reported on the short inorganic variants. Among the available time-resolved IR methodologies, two-dimensional infrared (2D IR) spectroscopy provides a unique route to obtain an in-depth understanding of the inorganic ligand−NC interactions. A particular mode of ligand−NC interaction is manifested as a symmetric peak in the FTIR spectrum. Due to the inherent heterogeneity in the NC ensemble, subensembles exist within each absorption band. These subensembles exchange on specific time scales (spectral diffusion) depending on the strength of interaction of the ligand to the NC surface (Figure 1a). The stronger the ligand−NC interaction, the slower the time scale (Figure 1b). The changes in the 2D IR line shapes can directly provide the spectral diffusion time scales and identify the relative strength of the ligand−NC interaction. Herein, we successfully demonstrate that the ligand dynamics time scales obtained from 2D IR spectroscopy in SCN^- capped CdS NCs quantitatively distinguish three distinct inorganic ligand−NC interactions within the heterogeneous ensemble.

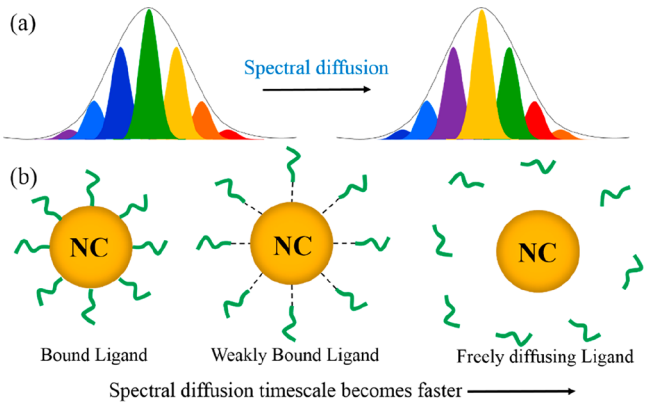

Figure 1. Schematic representations of (a) the exchanging heterogeneous subensembles (different colors) within a symmetric frequency distribution (solid black line representing an absorption band) leading to spectral diffusion and (b) the changes in the spectral diffusion time scales with variations in ligand−NC interactions.

For this work, oleic acid capped CdS NCs (CdS-OA) are synthesized with minor modifications to previously reported procedures.[28] CdS-OA in hexane is combined with a solution of ammonium thiocyanate (NH_4SCN) in DMF (detailed procedure in the Supporting Information) to exchange the organic ligands. After ligand exchange, ^1H NMR shows no characteristic peak for vinyl hydrogen of oleate around 5 to 6 ppm confirming full removal of oleate from the NCs surface (Figure S1). We choose the short SCN^- ligand because of its ability to form stable solution-phase NCs and its impressive electron mobility, which is required for optoelectronic applications.[15,29] Moreover, SCN^- is a highly sensitive local vibrational probe of the surface heterogeneity.[30,31] Figure 2a shows that the excitonic features of the CdS NCs were preserved after ligand exchange. The X-ray diffraction (XRD) pattern of the SCN^- capped CdS (CdS-SCN) was identical to that of CdS-OA (Figure 2b). HRTEM images of CdS NCs (Figure S2) before and after ligand exchange exhibit good crystallinity with well-defined lattice fringes. The size distributions of the NCs are shown in Figure 2c. In agreement with the previous literature, the fringe spacing and XRD correspond to (111), (220), and (311) planes of the zinc blend structure.[32] The XRD pattern reveals (111) to be the predominant facet.

The FTIR spectrum of the CdS-SCN in DMF shows an asymmetric peak in the CN stretch ($\bar{\nu}_{CN}$) region (Figure 2d) which could be fitted (Table S1) to two Gaussians centered at 2055 cm^{-1} ($\bar{\nu}_L$) and 2072 cm^{-1} ($\bar{\nu}_H$). The full width at half-maximum (fwhm) of the peaks at $\bar{\nu}_L$ and $\bar{\nu}_H$ are 16.5 and 14.6 cm^{-1}, respectively. In the absence of NCs, NH_4SCN shows a symmetric peak at 2055 cm^{-1} ($\bar{\nu}_F$) in DMF with a fwhm of 13.5 (Figures 2d). Previous studies of M^+SCN^- ($M = Li^+$, Na^+, Mg^{2+}) in different solvents reported a blue-shift in $\bar{\nu}_{CN}$ due to the formation of contact ion pairs.[33−38] Thus, the peaks at $\bar{\nu}_L$ and $\bar{\nu}_H$ in CdS-SCN can plausibly be assigned to the freely diffusing ligands and the ligands interacting with the NCs, respectively. However, these assignments based on peak positions are speculative. Further, it should be noted that although the presence of NCs makes the fwhm of the peak at $\bar{\nu}_L$ larger by 3 cm^{-1} than that of the peak at $\bar{\nu}_F$ (Table S1), the origin of this broadening cannot be explained from FTIR results.

We have acquired 2D IR spectra of CdS-SCN at different time delays (T_w) to obtain a detailed understanding of the ligand−NC interactions. A typical 2D IR spectrum consists of a peak pair corresponding to ground-state bleach and stimulated emission (blue peak, $v = 0$ to $v = 1$) and excited-state absorption (red peak, $v = 1$ to $v = 2$) separated by vibrational anharmonicity. The existence of multiple binding modes introduces multiple overlapping peak pairs (2D IR) in the spectra. The 2D IR spectrum shows two peak pairs (Figure 3, left column), with the blue peaks centered at frequencies corresponding to the FTIR peak positions ($\bar{\nu}_L$ and $\bar{\nu}_H$) and the red peaks shifted along the detection axis by the respective anharmonicities. The spectral diffusion (within each peak) lowers the diagonal tilt of the peaks with increasing T_w without changing the peak positions (white lines in Figure 3). The spectral diffusion time scales are quantified using center line slope (CLS) formalism where the inverse of the T_w-dependent white lines' slopes are fitted to exponential decays.[39] We have performed additional control experiments and analyses in the absence of NCs on NH_4SCN in DMF (Figure 3, right column).

The CLS of the peak at $\bar{\nu}_H$ fits well to a single exponential decay indicating that the spectral diffusion with this ligand population happens at a 114 ps time scale (Figure 4a). The CLS of the peak at $\bar{\nu}_L$ shows a biexponential decay, consisting of two decay time scales, 5 and 39 ps (Figure 4a). The faster (5 ps) time scale shows an excellent agreement with that obtained from the CLS of the peak ($\bar{\nu}_F$) in the absence of NCs, thereby confirming the existence of freely diffusing ligands. It is worth mentioning that the freely diffusing ligands can be paired with the NH_4^+ countercation. A previous study reported a much faster spectral diffusion in DMF (1 ps), albeit using transition metal carbonyl as the vibrational probe.[40] A future study involving variation in the cation size/charge density can provide a clearer picture. Direct binding to the NC surface should restrict the ligand movement and slow down the spectral diffusion. Thus, the slowest time scale corresponding

https://doi.org/10.1021/acs.jpclett.2c00493
J. Phys. Chem. Lett. 2022, 13, 3059−3065

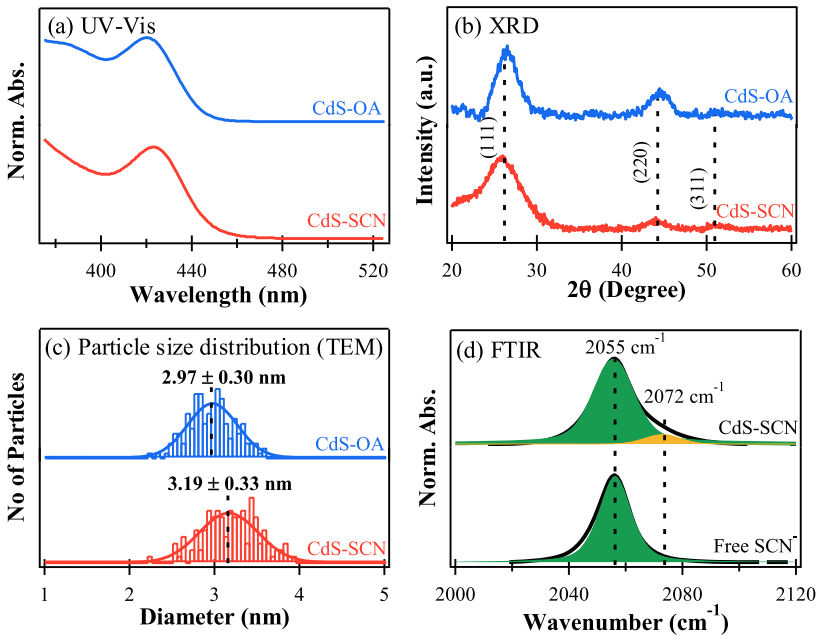

Figure 2. (a) UV−vis absorption spectra, (b) XRD patterns, and (c) particle size distributions obtained from HRTEM analysis of CdS NCs before (blue) and after (red) ligand exchange. (d) FTIR spectra of the nitrile stretch ($\bar{\nu}_{CN}$) of SCN^- in the presence (up) and absence (down) of NCs.

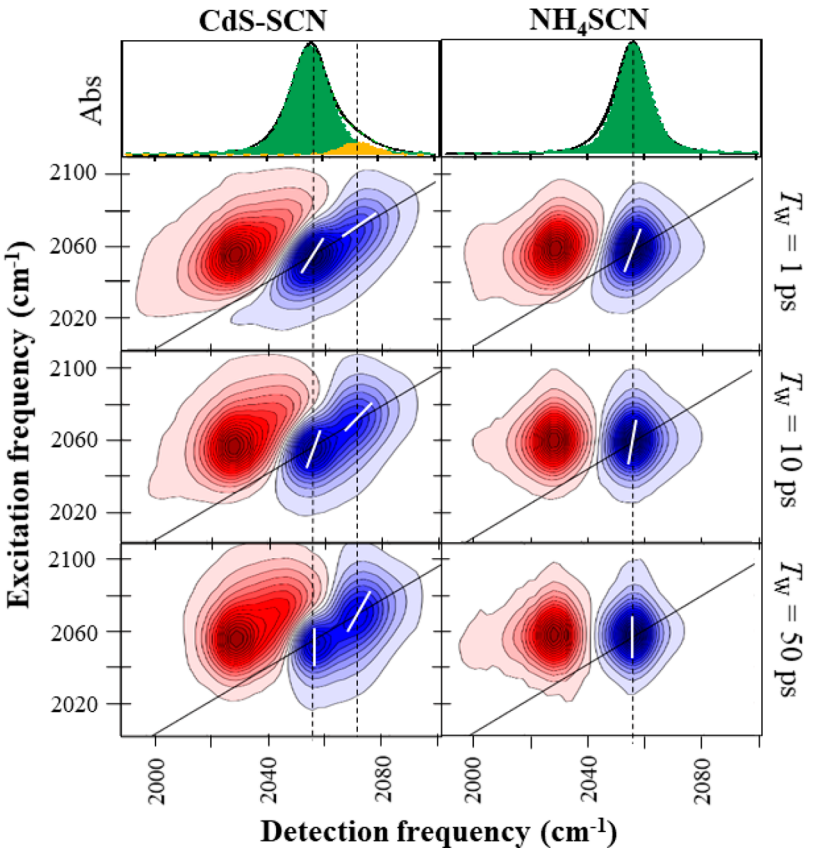

Figure 3. 2D IR spectra of CdS-SCN (left column) and NH_4SCN (right column) in DMF at three different waiting times (T_w). T_w increases from the top to the bottom along each column. FTIR spectra are shown at the respective top panels such that the peak positions of the FTIR and 2D IR spectra are vertically aligned.

to the peak at $\bar{\nu}_H$ arises due the strongly bound ligands. The negatively charged SCN^- likely binds (making X-type interaction) to the Cd-rich positively charged (111) surface, giving rise to this distinct ligand population. The intermediate time scale of 39 ps for the peak at $\bar{\nu}_L$ indicates a ligand population which is neither freely diffusing nor strongly bound to the NC surface. The ligand interacting weakly with the NCs would be less restricted than those bound strongly to the NCs

https://doi.org/10.1021/acs.jpclett.2c00493
J. Phys. Chem. Lett. 2022, 13, 3059−3065

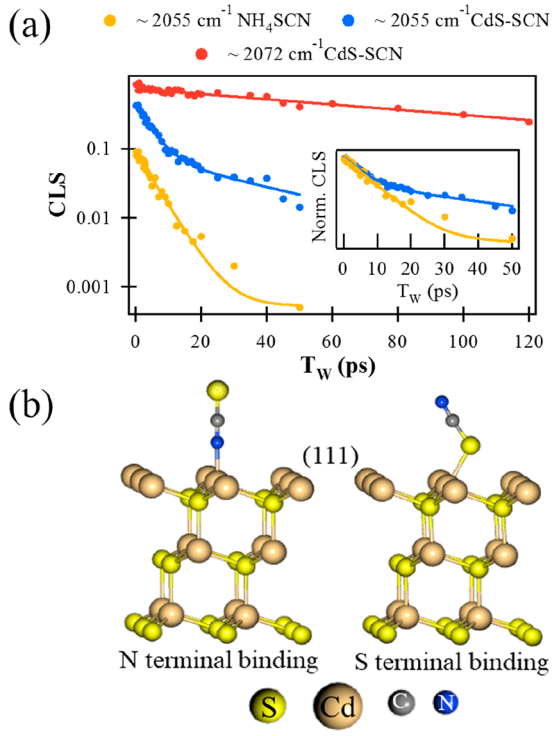

Figure 4. (a) T_w dependent CLS decays of the 2055 and 2072 cm^{-1} peaks of CdS-SCN are shown in blue and red, respectively. CLS decay of NH_4SCN (2055 cm^{-1}, yellow) has been appended for easy comparison with the blue decay. The *y*-axis is shown in log scale for clear visualization of the number of exponential decays. The inset represents the normalized CLS decays at 2055 cm^{-1} in the presence and absence of NCs. (b) Optimized slab structure of the N-terminated and S-terminated SCN^- capped (111) facet of the CdS crystal. We set $a = b = 8.40$ Å, $c = 60$ Å, and $\alpha = \beta = \gamma = 90°$ to construct the slab with chelating ligands. The vacuum spacing is about 45 Å, and thus the image effect is eliminated. The plane wave basis set is used with a kinetic energy cutoff of 25 Ry.

but would have slower dynamics than that of the freely diffusing ligands. The absorption of the weakly interacting ligands at a frequency similar to that of the freely diffusing ones makes these two ligand populations indistinguishable in the FTIR spectra. It has been previously reported that free thiocyanate anions cannot be spectrally distinguished from solvent separated ion pairs.[34,38] The only indication in the steady-state spectrum was the broadening of the peak at $\bar{\nu}_L$ as compared to that at $\bar{\nu}_F$. However, the ligand dynamics time scales obtained from 2D IR allows us to directly identify the variations in the ligand populations.

Interestingly, the freely diffusing ligands do not have any apparent interaction with the NCs, as indicated from the spectral diffusion time scales. We tried decreasing the ligand concentration during ligand exchange to remove the freely diffusing ligands. However, only a partial transfer of the NCs to the DMF phase was observed, which shows identical normalized FTIR spectra (Figure S3) irrespective of the ligand concentration. This result suggests that the free-diffusing ligands are an integral part of the heterogeneous NC system. A zeta potential value of −57.6 mV for CdS-SCN indicates that the ligands can provide electrostatic stabilization to the NCs. Our results demonstrate that the electrostatically bound ligands (39 ps time scale) are in dynamic equilibrium with the freely diffusing ligands (5 ps time scale). Thus, the free ligands could not be eliminated by reducing the ligand concentration during ligand exchange.

In addition to the distinct time scale upon binding to the NCs, the separation between the respective blue and red peaks (vibrational anharmonicity) for SCN^- is known to decrease with proximity to the cations.[41] The estimated anharmonicity (Table S1) is the lowest for the peak at $\bar{\nu}_H$, confirming that this peak arises from strongly bound ligands to the NCs. The anharmonicities of the weakly bound and the free ligands are the same, within the experimental error limit. Additional information is obtained from the amplitudes of the CLS decays (Figure 4a). Although the CLS value at $T_w = 0$ should be unity as no spectral diffusion is possible, it usually decreases from unity due to the presence of ultrafast homogeneous fluctuations. A larger decrease from unity at $T_w = 0$ indicates a larger homogeneous contribution to the line shape of the IR peak. It is intriguing to observe that the ultrafast fluctuations decrease with the increasing strength of ligand−NC interaction, thereby decreasing the homogeneous contribution to the IR line shape.

The ratio of the areas of the peaks at $\bar{\nu}_H$ and $\bar{\nu}_L$ is estimated to be 0.1 from the FTIR spectrum of CdS-SCN. In addition, the amplitudes of the biexponential CLS decay for the peak at $\bar{\nu}_L$ show that the weakly bound ligands contribute ∼20% while the rest comes from the freely diffusing ligands. Combining the two results, the population ratio of strongly bound ligands:weakly bound ligands:free ligands is estimated to be 1:2:7. A large fraction of free ligands is needed to stabilize the NCs as the free ligands are in dynamic equilibrium with both the strongly bound and the weakly interacting ligands. Although the IR spectra of CdS-SCN show two peaks arising from three overlapping transitions, a single peak in ^{13}C NMR[15] confirms the presence of a dynamic equilibrium between the three ligands populations. We therefore estimate a nanosecond time scale for the exchange process, i.e., faster than the NMR time scale and slower than picoseconds as no cross peaks from chemical exchange are seen up to 80 ps in 2D IR.

Although we have identified the strongly bound ligand population directly from the ligand dynamics time scales, the ambidentate SCN^- can bind to the positively charged (111) NC surface (X-type interaction) either through the sulfur (S) or the nitrogen (N) atom. Density functional theory (DFT) calculations on Cd^{2+}-SCN^- ion pairs (see Table S2 for calculated frequencies) predict a blue-shift in $\bar{\nu}_{CN}$ for SCN^- interacting with Cd^{2+} either through the S end or through the N end. To mimic the experimental condition, additional DFT calculations have been performed using Quantum-Expresso on the (111) facet of zinc-blende shaped CdS-NC. For simplification, a slab model has been used to optimize the NC structure.[42] PBE[43] was used as the exchange-correlation functional, and ultrasoft pseudopotentials[44] described the electron−ion interaction. Two different models considering the binding nature of SCN^- (S-bound and N-bound) have been constructed, and their optimized structures are presented in Figure 4b. Small fragments of the slabs were utilized to calculate the $\bar{\nu}_{CN}$ at the B3LYP/lanl2dz level of calculation with the Gaussian 16 package.[45] The calculated values of $\bar{\nu}_{CN}$ are presented in Table S2. A close resemblance of $\bar{\nu}_{CN}$ for the N-bound SCN^- (2079.36 cm^{-1}) to the (111) surface has been observed with an experimental band at 2072 cm^{-1}, indicating that the ligands are bound to the NC surface through the N atom, making an X type interaction with the (111) facet.

https://doi.org/10.1021/acs.jpclett.2c00493
J. Phys. Chem. Lett. 2022, 13, 3059−3065

Our results successfully demonstrate that the variations in the inorganic ligand−NC interactions at the NC surface can be successfully deciphered from the variations in the ligand dynamics (Figure 5). A unique spectral diffusion time scale,

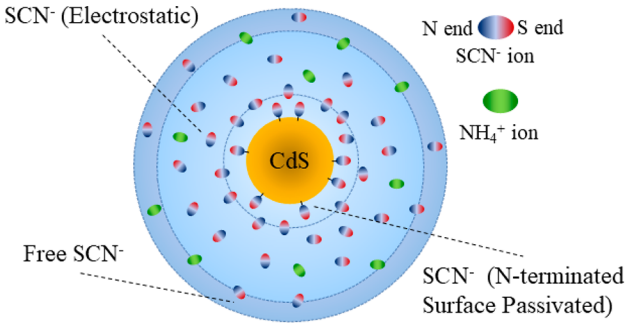

Figure 5. Schematic representation of different SCN^- populations in the CdS-SCN system.

associated with any ligand−NC interactions, depends on how strongly the ligand is interacting with the NC. A stronger interaction slows down the spectral diffusion such that the excitation and detection frequencies remain correlated for a longer time. We have identified three distinct populations of pseudohalide ligands—strongly bound, electrostatically interacting, and freely diffusing—in the CdS-SCN NCs. These ligand populations were found to be present in the NC system in the ratio 1:2:7. Furthermore, control experimental results indicate a dynamic equilibrium where all the three ligand populations exchange at nanosecond time scales. Interestingly, although the freely diffusing ligands do not apparently interact with NCs, the presence of the dynamic equilibrium between the various ligand populations make these free ligands an intrinsic part of the NC system. Results obtained from quantum chemical calculations show an excellent agreement with our 2D IR interpretations. In addition, the theoretical results indicate that the ambidentate SCN^- ligand binds through the N atom, making an X-type interaction with the NCs. This work demonstrates that 2D IR spectroscopy can directly provide a detailed molecular-level picture of how small inorganic ligands stabilize the NCs. In CdS-SCN, the stabilization of the NCs comes from passivating the surface charges through direct binding as well as electrostatic interaction. This study opens up a new avenue to investigate the interaction of small inorganic ligands with the NCs of varying shapes, sizes, and semiconductor materials.

■ ASSOCIATED CONTENT

Supporting Information

The Supporting Information is available free of charge at https://pubs.acs.org/doi/10.1021/acs.jpclett.2c00493.

Materials and methods, experimental details, material characterization of NCs (NMR and HR-TEM) and FTIR spectra, and results of quantum chemical calculations on NCs (PDF)

Transparent Peer Review report available (PDF)

■ AUTHOR INFORMATION

Corresponding Authors

Deborin Ghosh − *Physical and Materials Chemistry Division, National Chemical Laboratory (CSIR-NCL), Pune 411008, India*; Email: deborin88@gmail.com

Sayan Bagchi − *Physical and Materials Chemistry Division, National Chemical Laboratory (CSIR-NCL), Pune 411008, India; Academy of Scientific and Innovative Research (AcSIR), Ghaziabad 201002, India*; orcid.org/0000-0001-6932-3113; Email: s.bagchi@ncl.res.in

Authors

Samadhan H. Deshmukh − *Physical and Materials Chemistry Division, National Chemical Laboratory (CSIR-NCL), Pune 411008, India; Academy of Scientific and Innovative Research (AcSIR), Ghaziabad 201002, India*; orcid.org/0000-0002-0326-6125

Srijan Chatterjee − *Physical and Materials Chemistry Division, National Chemical Laboratory (CSIR-NCL), Pune 411008, India; Academy of Scientific and Innovative Research (AcSIR), Ghaziabad 201002, India*; orcid.org/0000-0001-9701-4158

Complete contact information is available at: https://pubs.acs.org/10.1021/acs.jpclett.2c00493

Notes

The authors declare no competing financial interest.

■ ACKNOWLEDGMENTS

S.B. thanks CSIR-NCL and SERB, India (EMR/2016/000576), for financial support. D.G. acknowledges SERB India (PDF/2018/000046) for financial support. The support and the resources provided by the "PARAM Brahma Facility" under the National Supercomputing Mission, Government of India, at the Indian Institute of Science Education and Research (IISER) Pune are gratefully acknowledge. S.H.D. acknowledges CSIR for a research fellowship. We would like to thank Dr. Arup Kumar Rath, Neha V. Dambhare, Debranjan Mandal, and Chandan Mahajan from CSIR-NCL, Pune, for their support in NC synthesis. We acknowledge Prof. Naresh Kumar Patwari from IIT Bombay for giving the access of Gaussian 16.

■ REFERENCES

(1) Gur, I.; Fromer, N. A.; Geier, M. L.; Alivisatos, A. P. Air-Stable All-Inorganic Nanocrystal Solar Cells Processed from Solution. *Science* **2005**, *310*, 462−465.

(2) Konstantatos, G.; Howard, I.; Fischer, A.; Hoogland, S.; Clifford, J.; Klem, E.; Levina, L.; Sargent, E. H. Ultrasensitive Solution-cast Quantum Dot Photodetectors. *Nature* **2006**, *442*, 180−183.

(3) Kovalenko, M. V.; Manna, L.; Cabot, A.; Hens, Z.; Talapin, D. V.; Kagan, C. R.; Klimov, V. I.; Rogach, A. L.; Reiss, P.; Milliron, D. J.; Guyot-Sionnnest, P.; Konstantatos, G.; Parak, W. J.; Hyeon, T.; Korgel, B. A.; Murray, C. B.; Heiss, W. Prospects of Nanoscience with Nanocrystals. *ACS Nano* **2015**, *9*, 1012−1057.

(4) Talapin, D. V.; Lee, J.-S.; Kovalenko, M. V.; Shevchenko, E. V. Prospects of Colloidal Nanocrystals for Electronic and Optoelectronic Applications. *Chem. Rev.* **2010**, *110*, 389−458.

(5) Gao, X.; Cui, Y.; Levenson, R. M.; Chung, L. W. K.; Nie, S. In Vivo Cancer Targeting and Imaging with Semiconductor Quantum Dots. *Nat. Biotechnol.* **2004**, *22*, 969−976.

(6) Howes, P. D.; Chandrawati, R.; Stevens, M. M. Colloidal Nanoparticles as Advanced Biological Sensors. *Science* **2014**, *346*, 1247390.

(7) Bell, A. T. The Impact of Nanoscience on Heterogeneous Catalysis. *Science* **2003**, *299*, 1688−1691.

(8) Hartley, C. L.; Kessler, M. L.; Dempsey, J. L. Molecular-Level Insight into Semiconductor Nanocrystal Surfaces. *J. Am. Chem. Soc.* **2021**, *143*, 1251−1266.

(9) Boles, M. A.; Ling, D.; Hyeon, T.; Talapin, D. V. The Surface Science of Nanocrystals. *Nat. Mater.* **2016**, *15*, 141−153.
(10) Anderson, N. C.; Hendricks, M. P.; Choi, J. J.; Owen, J. S. Ligand Exchange and the Stoichiometry of Metal Chalcogenide Nanocrystals: Spectroscopic Observation of Facile Metal-Carboxylate Displacement and Binding. *J. Am. Chem. Soc.* **2013**, *135*, 18536−18548.
(11) Noone, K. M.; Strein, E.; Anderson, N. C.; Wu, P.-T.; Jenekhe, S. A.; Ginger, D. S. Broadband Absorbing Bulk Heterojunction Photovoltaics Using Low-Bandgap Solution-Processed Quantum Dots. *Nano Lett.* **2010**, *10*, 2635−2639.
(12) Lu, H.; Joy, J.; Gaspar, R. L.; Bradforth, S. E.; Brutchey, R. L. Iodide-Passivated Colloidal PbS Nanocrystals Leading to Highly Efficient Polymer: Nanocrystal Hybrid Solar Cells. *Chem. Mater.* **2016**, *28*, 1897−1906.
(13) Seo, J.; Cho, M. J.; Lee, D.; Cartwright, A. N.; Prasad, P. N. Efficient Heterojunction Photovoltaic Cell Utilizing Nanocomposites of Lead Sulfide Nanocrystals and a Low-Bandgap Polymer. *Adv. Mater.* **2011**, *23*, 3984−3988.
(14) Itskos, G.; Papagiorgis, P.; Tsokkou, D.; Othonos, A.; Hermerschmidt, F.; Economopoulos, S. P.; Yarema, M.; Heiss, W.; Choulis, S. Size-Dependent Charge Transfer in Blends of PbS Quantum Dots with a Low-Gap Silicon-Bridged Copolymer. *Adv. Energy Mater.* **2013**, *3*, 1490−1499.
(15) Fafarman, A. T.; Koh, W.-k.; Diroll, B. T.; Kim, D. K.; Ko, D.-K.; Oh, S. J.; Ye, X.; Doan-Nguyen, V.; Crump, M. R.; Reifsnyder, D. C.; Murray, C. B.; Kagan, C. R. Thiocyanate-Capped Nanocrystal Colloids: Vibrational Reporter of Surface Chemistry and Solution-Based Route to Enhanced Coupling in Nanocrystal Solids. *J. Am. Chem. Soc.* **2011**, *133*, 15753−15761.
(16) Nag, A.; Kovalenko, M. V.; Lee, J.-S.; Liu, W.; Spokoyny, B.; Talapin, D. V. Metal-free Inorganic Ligands for Colloidal Nanocrystals: S^{2-}, HS^{-}, Se^{2-}, HSe^{-}, Te^{2-}, HTe^{-}, TeS_3^{2-}, OH^{-}, and NH_2^{-} as Surface Ligands. *J. Am. Chem. Soc.* **2011**, *133*, 10612−10620.
(17) Zhang, H.; Jang, J.; Liu, W.; Talapin, D. V. Colloidal Nanocrystals with Inorganic Halide, Pseudohalide, and Halometallate Ligands. *ACS Nano* **2014**, *8*, 7359−7369.
(18) De Roo, J.; Yazdani, N.; Drijvers, E.; Lauria, A.; Maes, J.; Owen, J. S.; Van Driessche, I.; Niederberger, M.; Wood, V.; Martins, J. C.; Infante, I.; Hens, Z. Probing Solvent - Ligand Interactions in Colloidal Nanocrystals by the NMR Line Broadening. *Chem. Mater.* **2018**, *30*, 5485−5492.
(19) Elimelech, O.; Aviv, O.; Oded, M.; Banin, U. A Tale of Tails: Thermodynamics of CdSe Nanocrystal Surface Ligand Exchange. *Nano Lett.* **2020**, *20*, 6396−6403.
(20) Zherebetskyy, D.; Scheele, M.; Zhang, Y.; Bronstein, N.; Thompson, C.; Britt, D.; Salmeron, M.; Alivisatos, P.; Wang, L.-W. Hydroxylation of the Surface of PbS Nanocrystals Passivated with Oleic Acid. *Science* **2014**, *344*, 1380−1384.
(21) Zhang, J.; Zhang, H.; Cao, W.; Pang, Z.; Li, J.; Shu, Y.; Zhu, C.; Kong, X.; Wang, L.; Peng, X. Identification of Facet-Dependent Coordination Structures of Carboxylate Ligands on CdSe Nanocrystals. *J. Am. Chem. Soc.* **2019**, *141*, 15675−15683.
(22) Fritzinger, B.; Capek, R. K.; Lambert, K.; Martins, J. C.; Hens, Z. Utilizing Self-Exchange to Address the Binding of Carboxylic Acid Ligands to CdSe Quantum Dots. *J. Am. Chem. Soc.* **2010**, *132*, 10195−10201.
(23) Giansante, C.; Infante, I. Surface Traps in Colloidal Quantum Dots: A Combined Experimental and Theoretical Perspective. *J. Phys. Chem. Lett.* **2017**, *8*, 5209−5215.
(24) Wang, Z.; Liu, T.; Long, X.; Li, Y.; Bai, F.; Yang, S. Understanding the Diverse Coordination Modes of Thiocyanate Anion on Solid Surfaces. *J. Phys. Chem. C* **2019**, *123*, 9282−9291.
(25) Pienpinijtham, P.; Han, X. X.; Ekgasit, S.; Ozaki, Y. Highly Sensitive and Selective Determination of Iodide and Thiocyanate Concentrations Using Surface-Enhanced Raman Scattering of Starch-Reduced Gold Nanoparticles. *Anal. Chem.* **2011**, *83*, 3655−3662.
(26) Leger, J. D.; Friedfeld, M. R.; Beck, R. A.; Gaynor, J. D.; Petrone, A.; Li, X.; Cossairt, B. M.; Khalil, M. Carboxylate Anchors Act as Exciton Reporters in 1.3 nm Indium Phosphide Nanoclusters. *J. Phys. Chem. Lett.* **2019**, *10*, 1833−1839.
(27) Kennehan, E. R.; Munson, K. T.; Doucette, G. S.; Marshall, A. R.; Beard, M. C.; Asbury, J. B. Dynamic Ligand Surface Chemistry of Excited PbS Quantum Dots. *J. Phys. Chem. Lett.* **2020**, *11*, 2291−2297.
(28) Murray, C. B.; Norris, D. J.; Bawendi, M. G. Synthesis and Characterization of Nearly Monodisperse CdE (E = Sulfur, Selenium, Tellurium) Semiconductor Nanocrystallites. *J. Am. Chem. Soc.* **1993**, *115*, 8706−8715.
(29) Sun, B.; Voznyy, O.; Tan, H.; Stadler, P.; Liu, M.; Walters, G.; Proppe, A. H.; Liu, M.; Fan, J.; Zhuang, T.; Li, J.; Wei, M.; Xu, J.; Kim, Y.; Hoogland, S.; Sargent, E. H. Pseudohalide-Exchanged Quantum Dot Solids Achieve Record Quantum Efficiency in Infrared Photovoltaics. *Adv. Mater.* **2017**, *29*, 1700749.
(30) Wu, B.; Breen, J. P.; Xing, X.; Fayer, M. D. Controlling the Dynamics of Ionic Liquid Thin Films via Multilayer Surface Functionalization. *J. Am. Chem. Soc.* **2020**, *142*, 9482−9492.
(31) Kim, H.; Cho, M. Infrared Probes for Studying the Structure and Dynamics of Biomolecules. *Chem. Rev.* **2013**, *113*, 5817−5847.
(32) Kumar, N.; Alam, F.; Dutta, V. Photoluminescence Study of Oleic Acid Capped and Hexanoic Acid Washed CdS Quantum Dots. *RSC Adv.* **2016**, *6*, 28316−28321.
(33) Yuan, R.; Yan, C.; Fayer, M. Ion−Molecule Complex Dissociation and Formation Dynamics in LiCl Aqueous Solutions from 2D IR Spectroscopy. *J. Phys. Chem. B* **2018**, *122*, 10582−10592.
(34) Lee, K.-K.; Park, K.-H.; Kwon, D.; Choi, J.-H.; Son, H.; Park, S.; Cho, M. Ion-pairing Dynamics of Li^+ and SCN^- in Dimethylformamide Solution: Chemical Exchange Two-dimensional Infrared Spectroscopy. *J. Chem. Phys.* **2011**, *134*, 064506.
(35) Firman, P.; Xu, M.; Eyring, E. M.; Petrucci, S. Thermodynamics of Dimerization of Sodium Thiocyanate in Some Acyclic Polyethers Studied by Infrared Spectroscopy. *J. Phys. Chem.* **1992**, *96*, 8631−8639.
(36) Saar, D.; Petrucci, S. Infrared and Ultrasonic Spectra of Sodium Thiocyanate and Lithium Thiocyanate in Tetrahydrofuran. *J. Phys. Chem.* **1986**, *90*, 3326−3330.
(37) Sun, Z.; Zhang, W.; Ji, M.; Hartsock, R.; Gaffney, K. J. Contact Ion Pair Formation between Hard Acids and Soft Bases in Aqueous Solutions Observed with 2DIR Spectroscopy. *J. Phys. Chem. B* **2013**, *117*, 15306−15312.
(38) Park, S.; Ji, M.; Gaffney, K. J. Ligand Exchange Dynamics in Aqueous Solution Studied with 2DIR Spectroscopy. *J. Phys. Chem. B* **2010**, *114*, 6693−6702.
(39) Kwak, K.; Park, S.; Finkelstein, I. J.; Fayer, M. D. Frequency-frequency Correlation Functions and Apodization in Two-dimensional Infrared Vibrational Echo Spectroscopy: A New Approach. *J. Chem. Phys.* **2007**, *127*, 124503.
(40) Dunbar, J. A.; Arthur, E. J.; White, A. M.; Kubarych, K. J. Ultrafast 2D-IR and Simulation Investigations of Preferential Solvation and Cosolvent Exchange Dynamics. *J. Phys. Chem. B* **2015**, *119*, 6271−6279.
(41) Roy, V. P.; Kubarych, K. J. Interfacial Hydration Dynamics in Cationic Micelles Using 2D-IR and NMR. *J. Phys. Chem. B* **2017**, *121*, 9621−9630.
(42) Giannozzi, P.; Baroni, S.; Bonini, N.; Calandra, M.; Car, R.; Cavazzoni, C.; Ceresoli, D.; Chiarotti, G. L.; Cococcioni, M.; Dabo, I.; Dal Corso, A.; de Gironcoli, S.; Fabris, S.; Fratesi, G.; Gebauer, R.; Gerstmann, U.; Gougoussis, C.; Kokalj, A.; Lazzeri, M.; Martin-Samos, L.; Marzari, N.; Mauri, F.; Mazzarello, R.; Paolini, S.; Pasquarello, A.; Paulatto, L.; Sbraccia, C.; Scandolo, S.; Sclauzero, G.; Seitsonen, A. P.; Smogunov, A.; Umari, P.; Wentzcovitch, R. M. QUANTUM ESPRESSO: A Modular and Open-source Software Project for Quantum Simulations of Materials. *J. Phys.: Condens. Matter* **2009**, *21*, 395502.
(43) Perdew, J. P.; Burke, K.; Ernzerhof, M. Generalized Gradient Approximation Made Simple. *Phys. Rev. Lett.* **1996**, *77*, 3865−3868.

https://doi.org/10.1021/acs.jpclett.2c00493
J. Phys. Chem. Lett. 2022, 13, 3059−3065

(44) Vanderbilt, D. Soft Self-consistent Pseudopotentials in a Generalized Eigenvalue Formalism. *Phys. Rev. B* **1990**, *41*, 7892−7895.
(45) Frisch, M. J.; Trucks, G. W.; Schlegel, H. B.; Scuseria, G. E.; Robb, M. A.; Cheeseman, J. R.; Scalmani, G.; Barone, V.; Petersson, G. A.; Nakatsuji, H.; Li, X.; Caricato, M.; Marenich, A. V.; Bloino, J.; Janesko, B. G.; Gomperts, R.; Mennucci, B.; Hratchian, H. P.; Ortiz, J. V.; Izmaylov, A. F.; Sonnenberg, J. L.; Williams-Young, D.; Ding, F.; Lipparini, F.; Egidi, F.; Goings, J.; Peng, B.; Petrone, A.; Henderson, T.; Ranasinghe, D.; Zakrzewski, V. G.; Gao, J.; Rega, N.; Zheng, G.; Liang, W.; Hada, M.; Ehara, M.; Toyota, K.; Fukuda, R.; Hasegawa, J.; Ishida, M.; Nakajima, T.; Honda, Y.; Kitao, O.; Nakai, H.; Vreven, T.; Throssell, K.; Montgomery, J. A., Jr.; Peralta, J. E.; Ogliaro, F.; Bearpark, M. J.; Heyd, J. J.; Brothers, E. N.; Kudin, K. N.; Staroverov, V. N.; Keith, T. A.; Kobayashi, R.; Normand, J.; Raghavachari, K.; Rendell, A. P.; Burant, J. C.; Iyengar, S. S.; Tomasi, J.; Cossi, M.; Millam, J. M.; Klene, M.; Adamo, C.; Cammi, R.; Ochterski, J. W.; Martin, R. L.; Morokuma, K.; Farkas, O.; Foresman, J. B.; Fox, D. J. *Gaussian 16*, Revision A.03; Gaussian, Inc.: Wallingford, CT, 2016.

https://doi.org/10.1021/acs.jpclett.2c00493
J. Phys. Chem. Lett. 2022, 13, 3059−3065